Research article

Deciphering m6A dynamics at a single-base level during planarian anterior-posterior axis specification

Liqian Chen [a,1], Hui Zhen [a,1], Zixin Chen [a], Mujie Huang [a], Daniel W. Mak [b], Wei Jin [a], Yuxiu Zou [a], Mingjie Chen [c], Mingyue Zheng [a], Qingqiang Xie [a], Zhongjun Zhou [b,*], Guoxiang Jin [a,*]

[a] *Guangdong Cardiovascular Institute, Medical Research Institute, Guangdong Provincial Geriatrics Institute, Guangdong Provincial People's Hospital (Guangdong Academy of Medical Sciences), Southern Medical University, Guangzhou 510080, China*
[b] *School of Biomedical Sciences, LKS Faculty of Medicine, The University of Hong Kong, Hong Kong, China*
[c] *Shanghai NewCore Biotechnology Co., Ltd., Room 309, Building C, No.154, Lane 953, Jianchuan Road, Minhang District, Shanghai, China*

ARTICLE INFO

ABSTRACT

Background: The establishment of the anterior-posterior (A-P) axis is a crucial step during tissue repair and regeneration. Despite the association reported recently of N^6-methyladenosine (m6A) with regeneration, the mechanism underlying the regulation of m6A in A-P axis specification during regeneration remains unknown. Herein, we deciphered the m6A landscape at a single-base resolution at multiple time points during A-P axis regeneration and constructed the *de novo* transcriptome assembly of the *Dugesia japonica* planarian.
Results: Immunofluorescence staining and comparative analysis revealed that m6A is widespread across the planarian and dynamically regulated during regeneration along the A-P axis, exhibiting a strong spatiotemporal feature. The resulting datasets of m6A-modified genes identified 80 anterior-specific genes and 13 posterior-specific genes, respectively. In addition, we showed that YTHDC1 serves as the primary m6A reader to be involved in the m6A-mediated specification of A-P axis during regeneration in *Dugesia japonica* planarian.
Conclusions: Our study provides an RNA epigenetic explanation for the specification of the A-P axis during tissue regeneration in planarian.

1. Introduction

Regeneration involves the replacement of missing organs, appendages, or large body regions. The specification of anterior-posterior (A-P) axis is a fundamental and complex patterning process that sets up the embryonic polarity and shapes the regeneration organism [1,2]. During the A-P axis specification, genetic programs (and morphogenetic movements) are spatiotemporally controlled and coordinated in a precise manner by the integration of distinct signaling pathways. Moreover, molecular genetic studies have revealed that numerous embryonic patterning genes indeed play a role in instructing tissue regeneration [3]. While these studies mainly focused on the role of specific "positional control genes" (PCGs) in planarian regeneration, the molecular mechanisms underpinning their expression and maintenance are still poorly understood. Genes with regional expression that are associated with a patterning RNAi phenotype are predicted to be PCGs [4]. Rapid regeneration of PCGs expressing regions is a key step in planarian regeneration [3]. Unexpectedly, the cells expressing PCGs turned out to be muscle cells [4]. Subsequent single-cell RNA sequencing of muscle from multiple regions along the planarian A-P axis revealed that many additional genes display regional expression in muscle [5,6]. A fragment will regenerate the major PCG-expression regions within 48 h post-injury. After 72 h, specialized neoblast patterns also change in pre-existing tissue regions because of PCG domain re-scaling in muscle.

The anterior pole subsequently helps consolidate PCG changes and mediates continued PCG pattern re-establishment in the blastema [3]. Although originally studied in the context of development, epigenetic reprogramming is at the forefront of regenerative medicine and its mechanistic role in tissue regeneration are only beginning to be understood.

Epigenetic modifications, including both histone acetylation and DNA methylation [7–10], have been shown to promote transcriptional activation of multiple regeneration-associated genes (RAGs). Studies from recent years have revealed that epitranscriptomic regulation
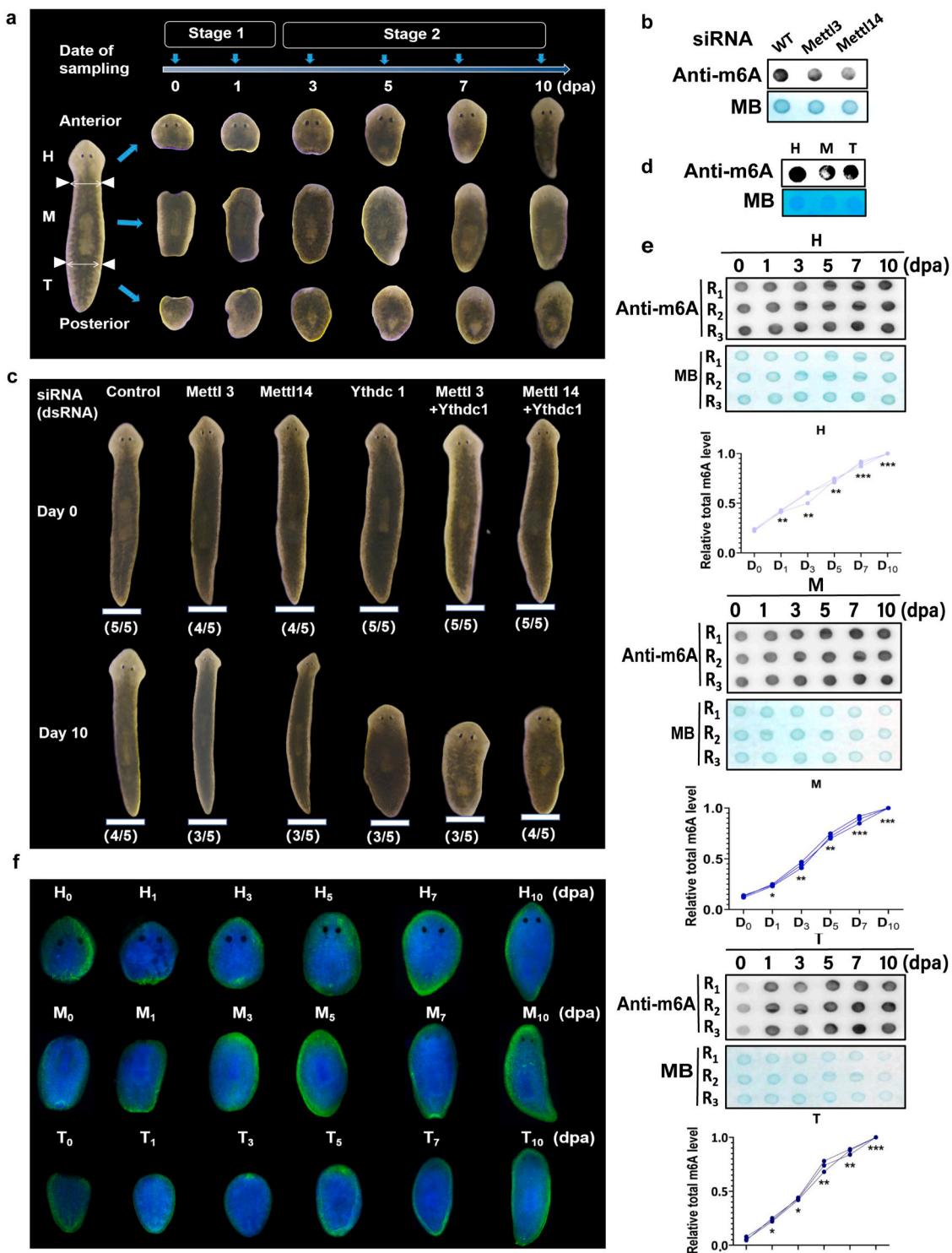
Fig. 1. Dynamic regulation of m6A during planarian regeneration. a, Schematic diagram of planarian regeneration study; b, Dot-blot assay of m6A content in the planarian after RNAi inhibition of *Mettl3* and *Mettl14* expression; c, Phenotype of planarian after RNAi inhibition of *Mettl3*, *Mettl14* and *Ythdc1* expression; d, Dot-blot assay of m6A content in the planarian head (H), trunk (M) and tail (T) fragments;e, Dot-blot assay and relative quantification of m6A content in the planarian head (H), trunk (M) and tail (T) fragments at each time point post amputation; f, The immunofluorescence staining of m6A , n = 4–6. H: Head , M: Trunk , T: Tail , dpa: days post amputation, R1: repetition 1, R2: repetition 2, R3:repetition 3. *: P < 0.05, **: P < 0.01, ***: P < 0.001.

involves highly complex and heterogeneous interactions, and thereby adding another layer of intricacy to the regulation the gene expression [11]. In particular, N^6-methyladenosine (m6A) has become a hotspot of RNA epigenetics research and has been shown to play an important and extensive role in post-transcriptional regulation of gene expression [12–14]. Found to be prevalent in eukaryotes, m6A is one of the most common internal mRNA modifications in mammals with tens of thousands of sites in the transcriptome and an occurrence frequency of 0.15–0.6 % of all adenosines [12–14]. m6A-mediated regulation is dependent on the recognition of m6A-binding proteins, which are represented by the YTH domain family and IGF2BP proteins [15,16]. YTHDC1 is one of the main readers expressed in some eukaryotes, such as honeybees [17]. In mammals, YTHDC1, as the only nuclear m6A reader, regulates the alternative polyadenylation (APA), alternative splicing (AS) and nuclear export of m6A-modified mRNAs in mouse oocytes [18]. Nevertheless, the exact role of m6A modification in planarian regeneration remains largely unknown. Similarly, whether YTHDC1 is the primary reader with the potential to regulate A-P axis specification also remains to be clarified.

Previous studies have provided important insights into the underlying molecular mechanisms of m6A-mediated regeneration at the cellular and tissue level, such as hematopoietic stem cells [19], mice nervous system [20], liver [21,22], muscle and muscle stem cells [23, 24]. It was only recently reported that m6A regulation indeed participates in the regeneration of the entire planarian organism [25]. However, the details of m6A's involvement in the specification of the A-P axis during planarian regeneration remains elusive.

In this study, we decipher the m6A landscape at the single-base level at multiple time points during the regeneration of the planarian along the A-P axis. We show that m6A modification occurs at specific regions of the mRNA, such as the coding sequence (CDS) and the 3′ untranslated region (3′ UTR) in the planarian tail and head fragments, respectively. We also uncover the associations between the m6A and the gene expression, and reveal that it is specific to the stage of regeneration and differs between the planarian fragments. Finally, we demonstrate that YTHDC1 is the primary m6A reader in planarian. Taken together, our study reveals that m6A epitranscriptomic marks are widespread and dynamically regulated during planarian regeneration of A-P axis specification with spatiotemporal features.

2. Results

2.1. Dynamic regulation of m6A during planarian regeneration

To characterize m6A modifications during planarian regeneration, we divided the regeneration into the first stage (from 0 to 1 days post amputation (dpa)), representing the wound healing stage which is initiated immediately after amputation, and the second stage (from 3, 5, 7 and 10 dpa), characterized by blastema (fragments regenerate missing body parts in outgrowths at the wound) development, growth and differentiation at the amputation site [3], as illustrated in Fig. 1a. To study the dynamic changes associated with m6A methylation, we collected planarian head, trunk and tail fragments at different stages during planarian regeneration.

m6A methylation is catalyzed by methyltransferase complex (MTC)

components including methyltransferase-like 3 (METTL3) and accessory proteins including METTL14, KIAA1429, WTAP, Hakai, RBM15/RBM15B, and ZC3H13 [26]. To investigate the potential function of m6A in planarian, we first examined m6A methyltransferase METTL3 and the accessory protein METTL14. Analysis of sequence similarity between planarian *Dugesia japonica* and human showed 39.68 %, 50.73 % and 44.58 % conservation in METTL3、METLL14 and YTHDC1, respectively (Table 1). Administration of double-stranded RNA (dsRNA) targeting the *Mettl3* and *Mettl14* resulted in a global decrease in m6A levels (Fig. 1b), indicating the conserved role of these proteins in m6A modification in planarian. The expression of the homologous m6A writer sub-units, *Mettl3* and *Mettl14*, were quantified using real-time polymerase chain reaction (qPCR). As shown in Fig. S1, the m6A writer subunits were dynamically expressed throughout the regeneration of the A-P axis after amputation (Fig. S1a). Silencing of the *Mettl3* and *Mettl14* did not result in a penetrant phenotype (Fig. 1c, Fig. S1b), that is consistent with a recent study showing that no significant phenotypic changes was found in the *Schmidtea mediterranea* planarian in response to depletion of most MTC components, though simultaneous knockdown of m6A reader proteins negatively affected the regeneration [25]. Therefore, we knocked down reader YTHDC1 and found that planarian showed a shorter body phenotype. The phenotype was aggravated after the simultaneous knockdown of writer and reader (Fig. 1c, Fig. S1b).

To understand a potential role for m6A in the specification of A-P axis, we collected the planarian head, trunk and tail fragments at different time point upon amputation (Fig. 1d). As shown in Fig. 1d, significant enrichment of m6A was found to be the highest in head followed by tail and trunk, respectively (Fig. 1d). Time point-based analysis on the relative level of m6A was increased for all three fragments upon amputation (Fig. 1e). In order to more intuitively observe the distribution of m6A in planarians, we detected the changes of m6A during planarian regeneration by immunofluorescence (Fig. 1f). According to the signal of fluorescence distribution, m6A is generally distributed in various cells of different segments of planarian, and the expression is relatively high in the subcutaneous cells (Fig. S2a). During regeneration, the m6A signal at the head and tail showed a trend of dynamic increase, and the fluorescence signal of the head is stronger than that of the tail (Fig. S2b). These results indicate that the m6A modification is dynamically regulated during planarian regeneration, therefore highlighting the importance of m6A abundance and its potential role as a regulatory factor during planarian regeneration.

2.2. Single-base profiling of m6A modifications during planarian regeneration

Given the environmental influence on the transcriptome and the dynamic nature of m6A modifications, the *de novo* transcriptome assembly was employed as a more suitable method in the analysis of gene expression in our samples. By employing Trinity assemblies, we showed that the unigenes length distribution were ~500 bp (Fig. 2a). The BUSCO assessment showed 84.3 % completeness of the assembled genome (Fig. 2b). We also observed a higher mapping rate in the *de novo* assembly when compared to publicly available planarian database (http://www.planarian.jp/download.html) (Fig. 2c). Since the

Table 1
Clustalw analyses the m6A methylation components between planarian and human.

Genesymbol	RefSeq	*De novo*	nr_id	Similarity
METTL3	NM_019852.5	TRINITY_DN30538_c0_g1*	CAC5412341.1	39.68 %
METTL14	NM_020961.4	TRINITY_DN1857_c0_g1*	CAE1267419.1	50.73 %
YTHDC1	NM_133370.4	TRINITY_DN383_c1_g1*	tr|T2M7P7|T2M7P7_HYDVU	44.58 %

* Since we are self-assembled transcript information, we have numbered and named each gene. For example, TRINITY_DN0_c1_g1_i1, where TRINITY represents the software name, DN0 represents the DeNovo number, c1 represents the assembled cluster number, g1 represents the gene number, and i1 represents the isoform number. Since several of these genes were obtained through the "nr" database alignment, the corresponding "nr" database number are shown for each of these genes.
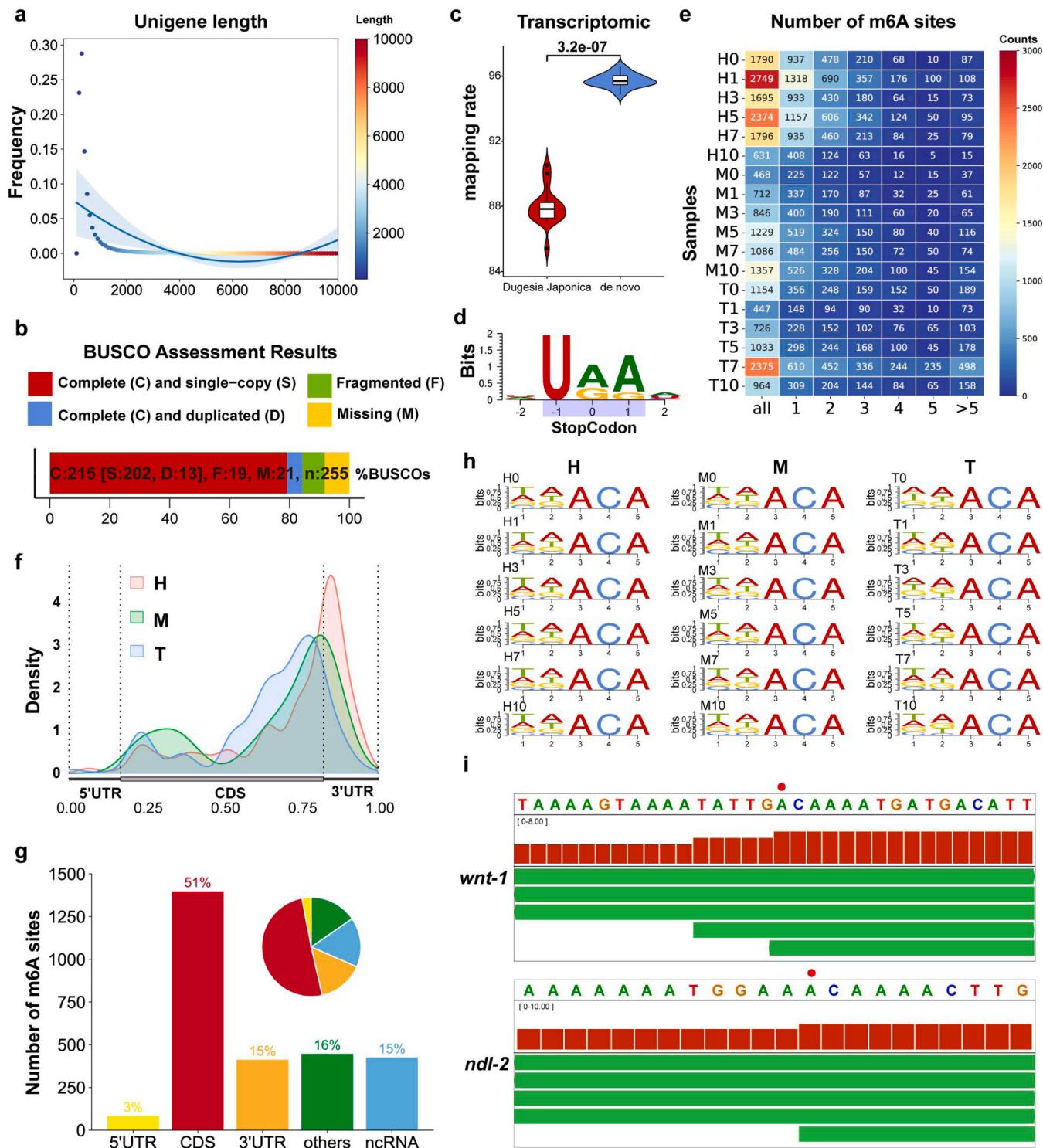
Fig. 2. Single-base resolution profiling of m6A reveals specific features of m6A modification during planarian regeneration. a, The fitted length distribution of assembled unigenes. X axis represents the unigene length and Y axis is the frequency; b, BUSCO assessment plot showing a 84.3 % C (complete); c, Violin plot comparison of the mapping rates between de novo assembled transcriptome and Dugesia japonica transcriptome; d, Transdecoder prediction of the stop codon motif such as the classical stop codons (UAG, UAA and UGA); e, Identification of the number of genes with m6A methylation sites in the planarian head (H), trunk (M) and tail (T) fragments at each time point post amputation; f, Distribution pattern of m6A sites in the different mRNA regions of the head, trunk and tail fragments, respectively; g, Pie chart and column diagram presentation of the proportion of m6A sites in five non-overlapping transcript segments in the 0 dpa samples; h, The conserved RRACH sequence motif of m6A modification identified in the planarian head (H), trunk (M) and tail (T) fragments at each time point post amputation; i, IGV display of a single m6A modification site in the wnt-1 and ndl-2 genes, which were also identified as PCGs. The red dot indicates the exact position of the m6A site.

transcriptomic stop codon position plays a key role in the functional analysis of m6A, we explored the position of the stop codons in the *de novo* transcriptome and found that they were enriched in the classical positions of UAA, UGA and UAG (Fig. 2d). These results showed that our transcriptome assembly can significantly improve the accuracy of the data analysis and is ideal in m6A functional and sequencing analysis (Table S2).

To map the changes in m6A level at a single-base resolution across the transcriptome during the transition from wound healing to regeneration in planarian, we next performed the m6A-REF-seq analysis [27]. Previous studies have shown that a reliance on an intermediate chemical reactions can result in the generation of false-positive or false-negative

results attributable to the incomplete labeling of the m6A [28]. To achieve increased accuracy in single-base m6A characterization, we calibrated the m6A-REF-seq analysis against a modification-free RNA library that resembles the endogenous transcriptome [29]. The schematic diagram of library construction processes is shown in Fig. S3, including RNA-seq, m6A-REF-seq and IVT library.

m6A sites were identified with different cutoffs from the planarian samples and those with high confidence sites (read count > 10, m6A ratio decrease > 0.1) were selected for further analysis as described previously (Fig. S4, Table S3) [27]. A total of 2749 genes were detected containing m6A modifications which varied in number between each planarian fragments and at different time point upon amputation
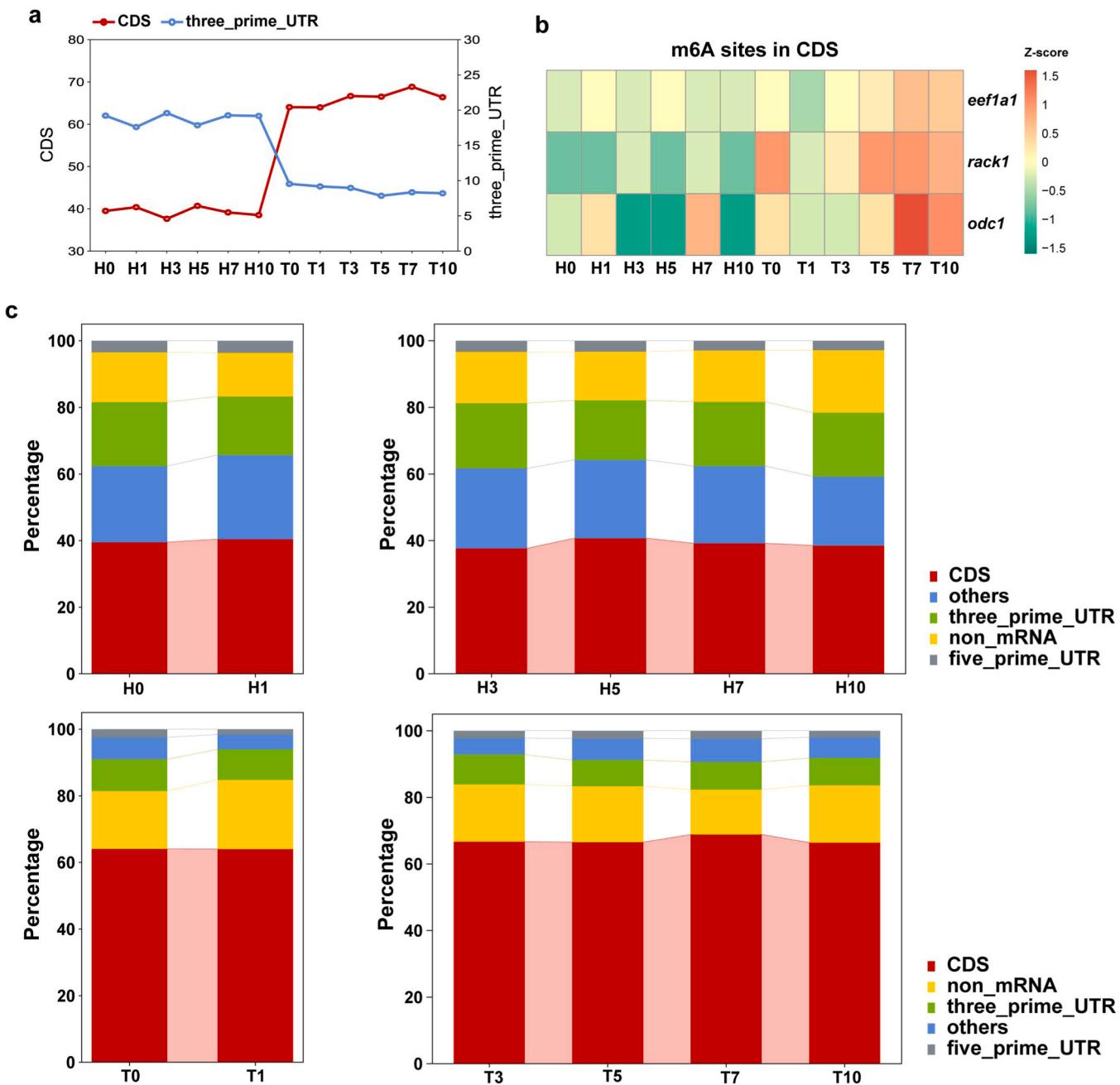
Fig. 3. Regional preference of the m6A distribution during A-P axis specification. a, Partition distribution of m6A sites in the different RNA transcriptome regions of the planarian head (H) and tail (T) fragments at each time point post amputation; b, Heat map of Z-score values representing m6A methylation levels in the CDS region of the regeneration-related genes *Eef1a-1*, *Rack-1*, *Odc-1*. Each row represents a gene, and each column represents either the head (H) or tail (T) fragment at a specific time point post amputation. The heatmap color range is from red for Z-score positive values to green for Z-score negative values. c, A cumulative bar graph comparing the distribution of m6A sites in the different RNA transcriptome regions of the head (H) and tail (T) fragments at each time point post amputation.

(Fig. 2e, Table S4). Because of the ability to detect m6A modifications at a single base level, we were able to distinguish genes that contained one to five m6A sites from those with more than five in each sample (Fig. 2e, Table S5.1–5.3).

Next, we investigated the distribution of differentially methylated m6A sites on a transcriptome-wide scale in the regenerating planarian. The transcripts were divided into 5′ UTR, CDS, 3′ UTR, non-coding RNA (ncRNA) and other regions. As shown in Figs. 2f-g, m6A sites identified were distributed in different regions and were especially enriched in the CDS and 3′ UTR regions, accounting for 51 % and 15 % of total m6A sites, respectively. Interestingly, m6A sites in the transcripts preferentially located in the 3′ UTR region at the head but in the CDS region at the tail (Fig. 2f). m6A enrichment analysis revealed a consensus RRACH (R is A/G and H is A/C/U) motif, which reinforced the authenticity of the data (Fig. 2h) and is consistent with previous findings in mammals, honeybees, drosophilas and even plants [12,17,31,32].

We next sought to determine what insights can be garnered by utilizing m6A-REF-seq to map m6A at the single base level that would otherwise have been missed should a low-resolution m6A-sequencing technique had been used instead. Indeed, a closer observation of some of the genes revealed that m6A modification can be detected at a precise location in the *wnt-1* and *ndl-2* gene sequences as shown in Fig. 2i. Finally, in order to more intuitively observe the proportion of m6A contained in each sample, we analyzed the percentage of the number of m6A modified transcripts in each stage, and the results further demonstrated the dynamic nature of m6A distribution during planarian regeneration (Fig. S4b). In brief, the single-base m6A landscape of the planarian regeneration provides a reference to which the dynamic changes in m6A modifications may be associated with planarian regeneration.

2.3. m6A constitutes region- and time-specific features during A-P axis specification

Based on the above analysis, the m6A sites identified in the head and tail fragments exhibited differential distribution preference in RNA (Fig. 2f). This implied a potential connection between the preferential distribution of m6A and A-P axis specification. Indeed, enrichment analysis of m6A modifications revealed that m6A were not randomly distributed, instead, predominantly enriched at the CDS region in the tail fragment and 3′ UTR region in the head fragment (Fig. 3a). For example, the m6A was enriched in CDS of *Eef1a-1*, *Rack-1*, and *Odc-1* genes in the tail (Fig. 3b). Given that these genes have been reported in cell growth and/or tissue development [33–35], their m6A modifications may be associated with the regeneration of anterior-facing wounds of the tail fragments. Also as we see , the differences in transcript region of m6A modifications in the head and tail modifications are present at day 0, so the main differences between CDS and 3′UTR are there already prior to regeneration and differences could be to due to differences in tissues. These results implied that m6A may regulate A-P axis specification through preferential distribution of m6A sites.

To investigate how m6A sites are regulated at the first and second regeneration stages upon amputation, the distribution of m6A during the two stages in both head and tail regeneration were analyzed. Notably, changes in m6A occurred in regions other than the CDS during the first regeneration stage (0–1 dpa). In contrast, m6A levels changed in all regions, including the CDS, during the second stage (3–10 dpa) of regeneration (Fig. 3c, Table S6.1–6.4). These results indicate that region- and time-specific features of m6A is attributable to the process of planarian A-P axis specification.

To identify the genes that are regulated by m6A modifications during A-P axis specification, different clusters of the samples across all 6 time points post amputation revealed that m6A-modified genes could indeed distinguish the first and second stage of regeneration by two and four different molecular subclusters, respectively (Fig. 4a , Table S7). These clusters are sorted according to the m6A ratio value. Each row is an m6A

methylation site, and each column represents a different sample. Next, GO functional enrichment analyses were performed on above clusters and found that m6A-modified mRNAs have vital functions in multiple biological processes, including post-transcriptional and translational regulation, such as mRNA stabilization, RNA splicing, mRNA poly(A) tail shortening, protein stabilization, translational elongation, translational initiation, etc. (Fig. 4b). These results highlight the dynamic regulation of m6A modification in mRNA during A-P axis specification and suggested that the rewiring of m6A modification may modulate gene expression which in turn facilitates the transition between different stages during regeneration.

## 2.4. Transcriptional regulation pattern of m6A during A-P axis specification

To investigate the regulatory effect of m6A on gene transcription during A-P axis specification, we first compared the integrated expression of genes containing m6A and those without m6A at different stages of regeneration. The violin plots showed that the expression of m6A-modified genes was more abundant in both the head and tail fragments as well as in both the first and second stages of regeneration (Fig. 5a). These results indicated that transcripts containing m6A have a higher expression level than those without m6A in planarian fragments. However, this integrated expression analysis did not enable us to find any differences in the regulation of m6A during A-P axis specification.

To further evaluate the relationship between m6A modification and transcription, we performed a stepwise analysis of m6A-REF-seq and RNA-seq datasets by classifying genes into upregulated or downregulated genes during regeneration. Notably, genes with up-regulated m6A accounted for the highest proportion of the regulated genes at the first stage of regeneration in the head fragment (Fig. 5b, Table S8). This cluster of genes displayed a positive correlation between m6A and gene expression (both were upregulated). However, genes with downregulated m6A and increased expression were predominant in the second stage of regenerating head fragment (Fig. 5b, Table S8). Conversely, the first stage of the regenerating tail exhibited a negative correlation as represented by downregulated m6A methylation and upregulated gene expression, whereas the second stage exhibited a positive correlation (both m6A methylation and gene expression were upregulated) (Fig. 5b, Table S8). These results further support the correlation between m6A modification and planarian A-P axis specification during regeneration, through stage-dependent transcriptional regulation.

2.5. Potential targets of m6A-modified genes during A-P axis specification

Given the distinct gene regulation by m6A methylation during regeneration between planarian head and tail fragments, we sought to assess which m6A-modified genes control A-P axis specification in these planarian fragments. After amputation, head and tail fragments expressed anterior and posterior PCGs, respectively (Fig. 6a, Table S9). However, the mapping of the m6A modification to these PCGs unexpectedly revealed that m6A methylation was rare and that only a few of these PCGs (eg. *ndl-1*, *prep*, *wntP-2*) exhibited this epitranscriptomic modification. Moreover, a comparison between the expression levels of these m6A-modified PCGs revealed no obvious correlation between m6A modification and gene expression either in head or in tail regeneration (Fig. 6b). These findings indicate that the m6A modification may not directly target the classical PCGs, instead target other group of genes. Although PCGs may not be the direct target of m6A regulatory pathways involved in regeneration in our data, it cannot be ruled out that PCGs serve as upstream regulatory proteins related to m6A, so it is an interesting question to further explore the relationship between PCGs and m6A.

To identify the potential targets of m6A-modified genes that are associated with A-P axis specification, we first selected the fragment-specific m6A-modified genes at each time point upon amputation
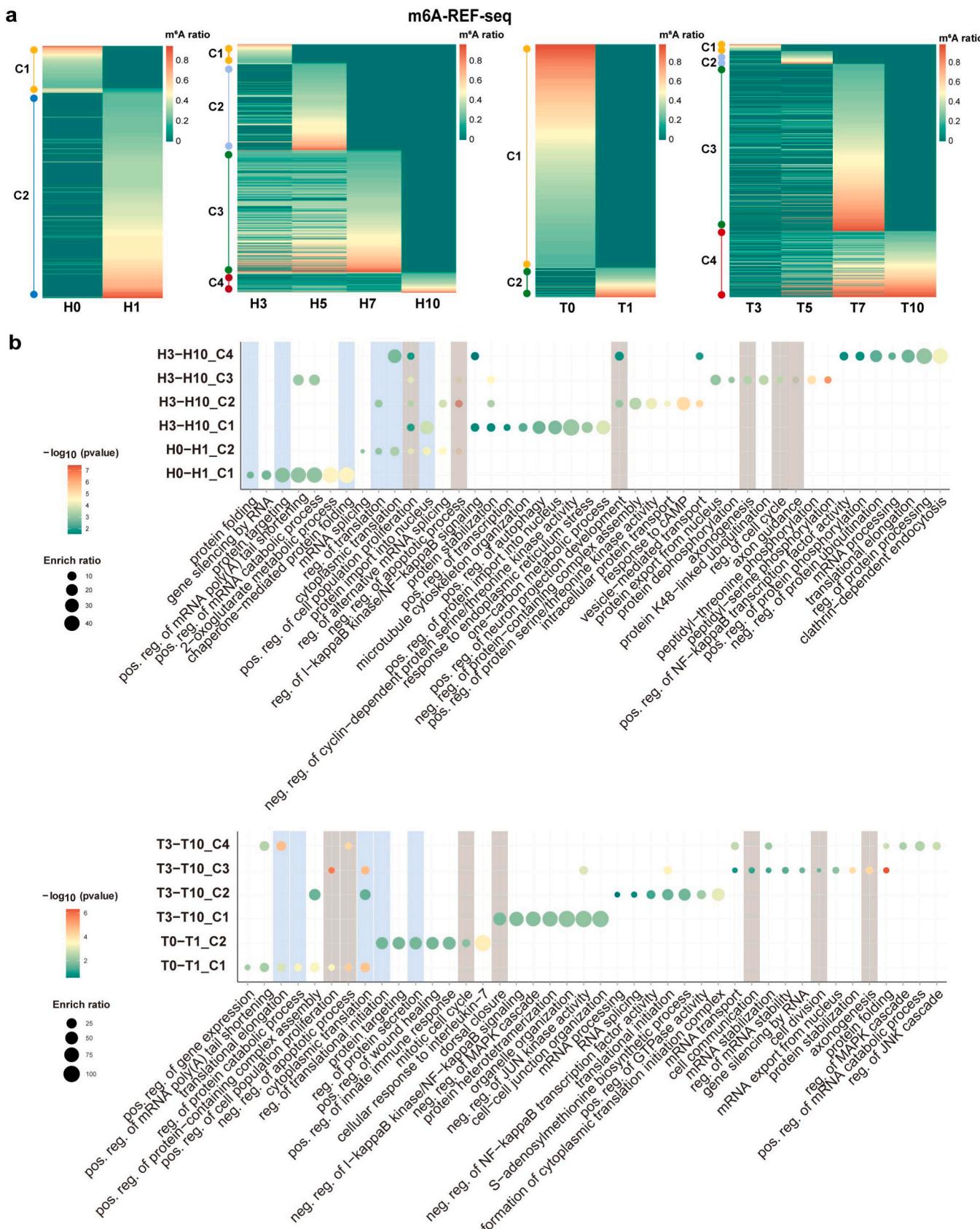
Fig. 4. Correlation between m6A modifications and gene expression patterns at each stage of the planarian A-P axis specification. a, Cluster heatmap analysis of m6A-modified genes in planarian head (H) and tail (T) fragments. Rows and columns data were normalized and the row data were clustered by euclidean; b, GO analysis of the gene clusters in the first (0–1 dpa) and second stage [3–10] of planarian head (H) and tail (T) regeneration. The bubble color gradient ranked from red to green according to -log10(q-value), and the bubble size ranked according to the number of genes in the enriched terms. C1: cluster1, C2: cluster2, C3: cluster3, C4: cluster4. Blue highlights indicate functions related to translational regulation and gray highlights those related to regeneration.
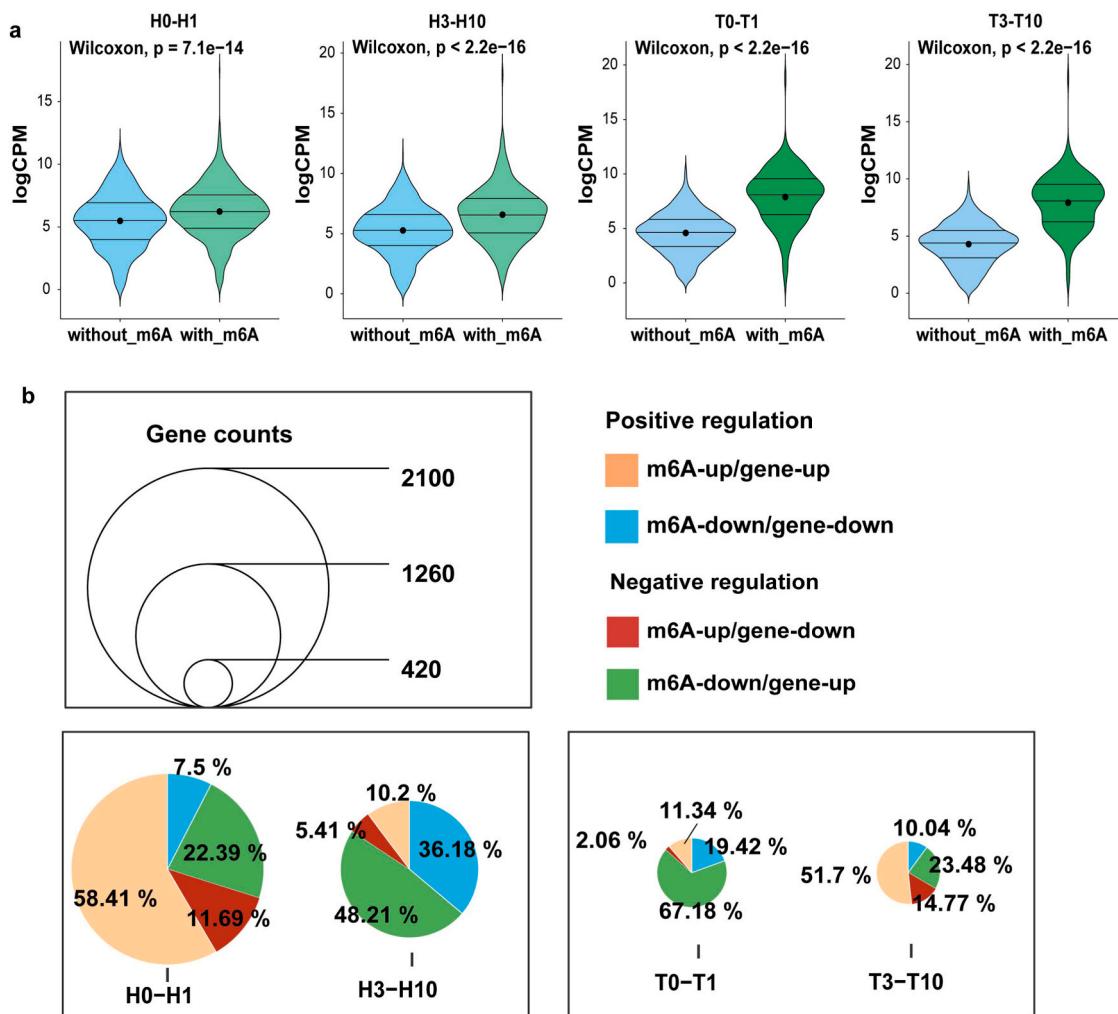
Fig. 5. Transcriptional regulation of m6A modification during A-P axis specification. a, Expression of genes with and without m6A modification during planarian regeneration, y-axis represents log2(CPM) of genes; b, The up panel circle diagram is a size scale facilitating the visualization of bottom panel. The size of the circle diagram means the displayed gene counts. Bottom panel, pie charts analysis of the proportion of m6A-modified genes with positive or negative correlated m6A methylation and transcript expression in the first (0−1) and second [3–10] stages of regeneration, whereby the size of the pie charts corresponds to the gene counts as shown in the circle diagram above.

(Fig. S5). Then, the intersection of specific m6A-modified genes between the regenerating head- and tail- at different time points post amputation were obtained to determine the corresponding m6A-modified gene clusters (Fig. 6c). As shown in Fig. 6, 80 and 13 m6A-modified genes were identified to be specifically expressed in the regenerating head and tail fragments, respectively (Fig. 6c, Table S10). We further analyzed and displayed the functional annotations related to these genes, and found that most of the genes were related to growth, morphogenesis and tissue regeneration(see Table S11). This suggests that related genes may respond to and be regulated by m6A signaling during planarian head and tail regeneration.

2.6. YTHDC1 as the primary m6A reader regulating in the A-P axis specialization

It is well-established that the effects of m6A within a given mRNA are conveyed by m6A readers in most organisms and cell types. Accordingly, we sought to determine the key m6A reader that can parse the different regulatory patterns at the A-P axis specification. Recent studies have shown that inhibition of both MTC-encoding genes and *ythdc-1* eliminated the ability of the animals to regenerate [25]. In some eukaryotes, such as honeybees, YTHDC1 is also a major reader expressed in various tissues. Our analysis also showed that YTHDC1 was the predominant

reader expressed in each fragment of the planarian *Dugesia japonica* strain, whereas the expression levels of other readers were below the detection threshold (Fig. S6). Sequence similarity of the YTHDC1 were compared between the planarian *Dugesia japonica* and human and 44.58 % of YTHDC1 were found to be conserved (Table 1).

In order to gain further insights into the mechanisms underlying YTHDC1-mediated transcriptional control during planarian regeneration, we performed the clustering of differently expressed genes using an unsupervised clustering algorithm implemented in the mfuzz program to identify sets of co-regulated genes with similar expression patterns throughout each time point after amputation [36]. This co-expression analysis yielded nine distinct clusters (Fig. 7a , Table S12). A focused heatmap of clusters containing the m6A reader gene, *ythdc1*, showed that diametrically opposed pattern of expressed genes between the head and tail fragments (Fig. 7b, Table S13). These results suggest different regulatory behaviors of YTHDC1 during A-P axis specification. These genes were enriched in functional annotation related to transcription regulation, cell proliferation, mRNA splicing, chromatin remodeling and morphological development (Fig. S7a).

We then further investigated the correlation between *ythdc1* expression and m6A-modified genes specific to head and tail. To visualize the distribution of YTHDC1 in planarian, we examined the expression changes during regeneration of head and tail by
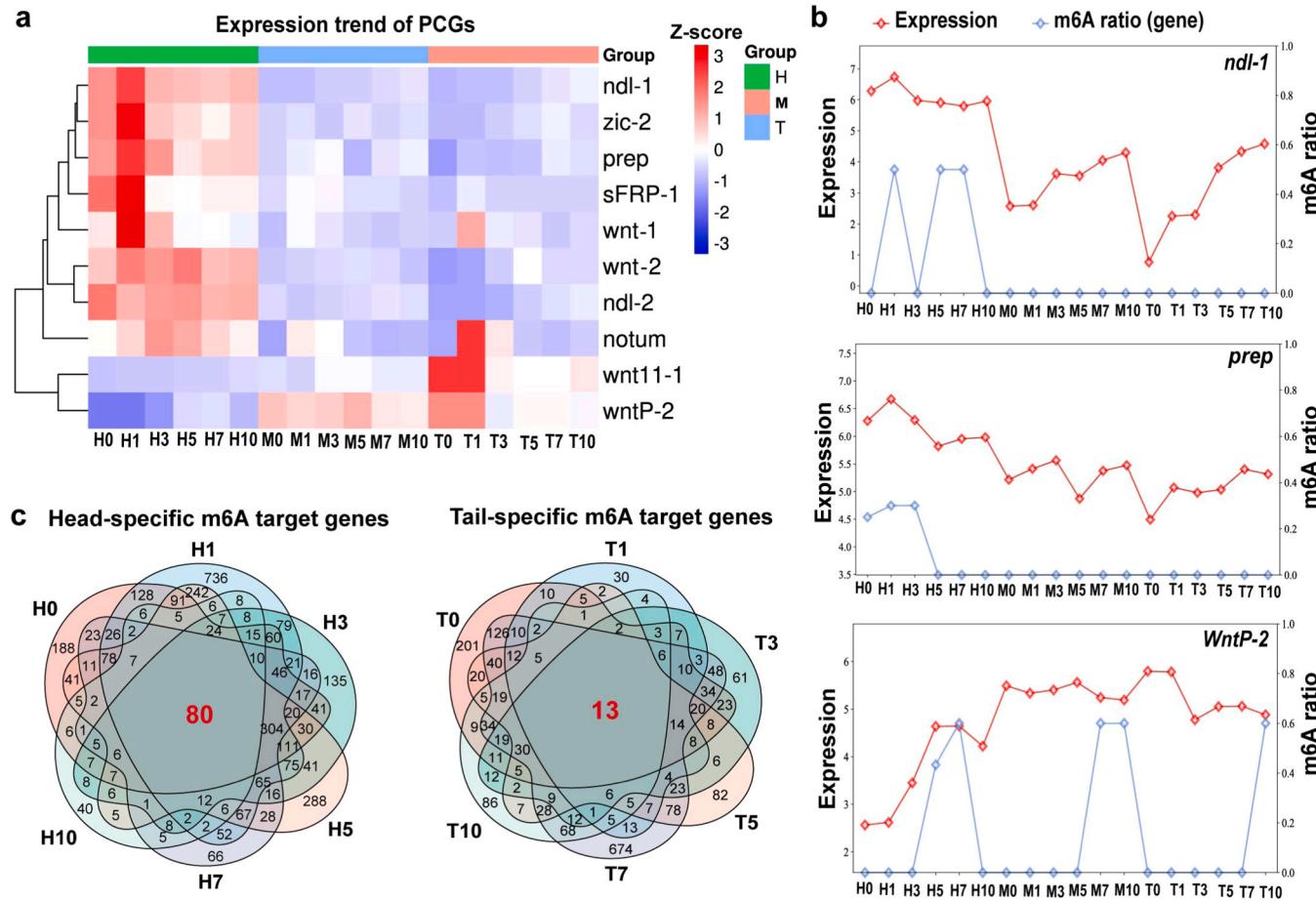
Fig. 6. Potential m6A-modified genes related to the specification of the A-P axis. a, Heat map of PCGs genes in the different planarian fragments during regeneration; b, Correlation of PCGs (*ndl-1*, *zic-2*, *prep*, *wntP-2*) expression and m6A density during planarian regeneration; c, Venn diagram analysis of the number of head and tail specific m6A-modified genes at the different time points post amputation.

immunofluorescence (Fig. 7c-d, Fig. S2a). It can be seen from the figure that YTHDC1 is expressed in different segments of planarian, and it is mainly expressed in the subcutaneous surface cells of planarian (Fig. S2a). The expression of YTHDC1 dynamically increased significantly with the progress of regeneration (Fig. S2c). In addition, we further observed the m6A read fluorescent protein METTL3 and METTL14 positioning, and found that the expression pattern of YTHDC1 is very similar to that of writer, which also illustrates the consistency of their regulatory functions (Fig. 7c-d, Fig. S2a,c). To further verify the importance of YTHDC1 for planarian head and tail specialization, we interfered with the expression of YTHDC1 and observed its changes during regeneration. The results showed that knockdown of YTHDC1 expression resulted in a significant lag in regeneration of the head and tail, but no significant effect on the trunk (Fig. 7e, Fig. S7b). Moreover, *ythdc1* gene exhibited a positive correlation with the head- and tail-specific m6A-modified genes in the first stage (0–1 dpa) of regeneration, as well as in the second stage (3, 5, 7 and 10 dpa) of head regeneration. In contrast, a negative correlation was observed between *ythdc1* and tail-specific m6A-modified genes in the second stage (3, 5, 7 and 10 dpa) (Fig. 7f, Table S14.1–14.2). These results imply that *ythdc1*, the major m6A reader in planarian, differentially regulated the expression of genes that are specific to the regeneration of either the planarian head or tail, and thereby establish the A-P axes in the regenerating planarian.

Lastly, we propose herein a model in which YTHDC1 binds to the m6A sites at the 3′ UTR and CDS region to regulate the regeneration of the head and tail related wounds, respectively (Fig. S7c). This conjecture provides an RNA epigenetic explanation for the specification of the A-P

axis during tissue regeneration.

3. Discussion

RNA m6A modification has been implicated in a myriad of roles in stem cell differentiation and tissue regeneration [20–25]. Despite of the essentiality of m6A methylation, the potential significance of RNA m6A modification in regeneration is not well understood. In this study, we provided the first transcriptome-wide characterization of m6A at a single base resolution in the regenerating planarian *Dugesia japonica*. We showed that m6A was highly specific in the planarian tissue with distinct patterns in different regions during the regeneration. This was associated with specific sets of gene expression to specify the regeneration towards opposite direction along A-P axis. The associations between m6A and gene expression was also specific to the stage of regeneration. In addition, YTHDC1 was found to be the primary reader in *Dugesia japonica* planarian. Collectively, our study revealed that m6A were widespread and dynamically regulated across the planarian during regeneration.

Our transcriptome-wide mapping utilized the m6A-sensitive RNA-endoribonuclease-facilitated sequencing method (m6A-REF-seq), an orthogonal method independent of m6A antibody, based on the recognition of RNA endonuclease MazF towards the m6A at the ACA motif. Though adopted by most current methods, detection of m6A by m6A antibodies suffers from the poor reproducibility and limited resolution (~100nt) [37], while the m6A-REF-seq could identify transcriptomic m6A sites and quantify the methylation level of m6A at the
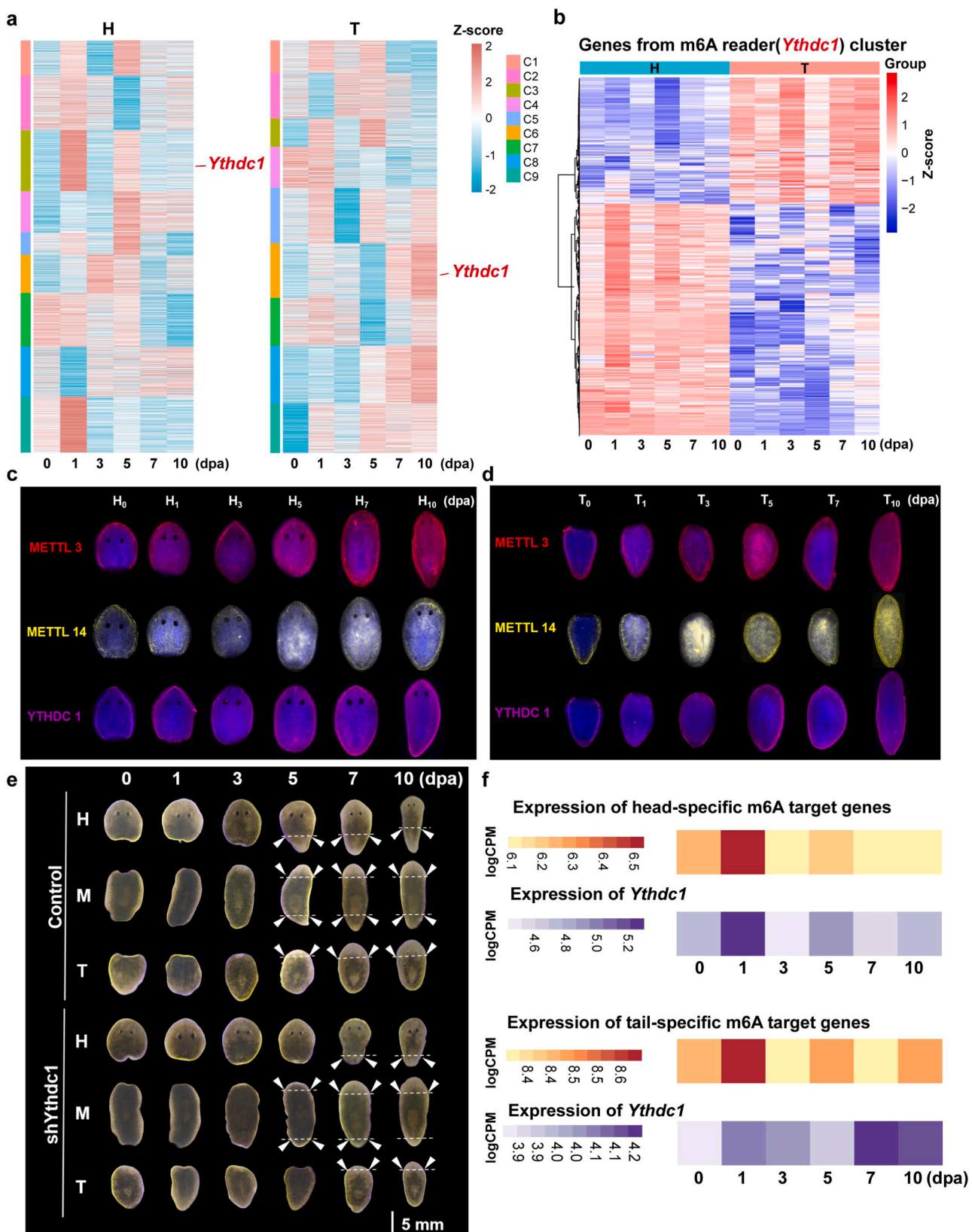
Fig. 7. YTHDC1 as the major m6A reader regulating the A-P axis specification. a, Heatmap of head (H) and tail (T) m6A-modified genes divided into nine clusters at the time points post amputation; b, Cluster heat map of head (H) and tail (T) m6A-modified genes in the m6A reader (*Ythdc1*) group at each time point post amputation. The color scale indicates the degree of correlation (blue, low correlation; red, high correlation); c-d, The immunofluorescence staining of YTHDC1, Mettl3 and Mettl14 during regeneration, n = 4–6; e, The interference phenotype of YTHDC1 during regeneration, the regenerated tissues were marked with a white curve with two arrows, n = 5; f, Correlation between Ythdc1 expression and head- and tail- specific m6A-modified genes at each time point post amputation.

single-nucleotide level [27,28].

Our analyses indicated that m6A represents a feature of the regenerating planarian with a high spatiotemporal specificity. For example, m6A enrichment in the CDS regions were found predominantly in the tail whereas the 3′ UTR region were mainly found in the head fragments. A recent study employing the antibody-dependent approach detects an increase in m6A sites in the CDS and 3′ UTR in the planarian *Schmidtea mediterranea* during the regeneration progression [25].

Previous studies have highlighted the tissue specificity of m6A peaks in ubiquitously expressed genes [25]. Here, we underscored the importance of the dynamic methylation in the regulation of stage-specific gene expression in planarian regeneration. m6A intensity and expression of the m6A-modified genes varied in different regions during regeneration. For example, genes with both up-regulated m6A and transcription accounted for the largest proportion in the first stage during head regeneration, while those with down-regulated m6A and up-regulated transcription represented the majority of the population in the second stage during head regeneration. In contrast, the majority of genes exhibited a negative correlation in the first stage of tail regeneration and a positive correlation in the second stage, between the m6A methylation and gene expression (Fig. 5b, Table S8). These findings implied that the regulatory effect of m6A may influence specification of a region along the A-P axis.

Recent studies have indicate that m6A modification of RNAs plays a pivotal role during planarian regeneration [25]. Planarian constitutively expresses dozens of local PCGs along different axis of the planarian, which drive the positional identity necessary for the guidance of tissue regeneration [7]. Intriguingly, we found that the m6A modification may not target the classical PCGs directly, suggesting that m6A regulates the A-P axis specification by means other than modulating PCGs during Regeneration.

In line with a previous study in the planarian *Schmidtea mediterranea* [25], we have identified YTHDC1 as the primary m6A reader in the planarian *Dugesia japonica*. YTHDC1 was expressed across different cell types and stages in lineage differentiation and the inhibition of its expression resulted in impaired regeneration [25]. Interestingly, our study indicated that YTHDC1 may have different binding preferences to the m6A sites between the anterior and posterior regions. The YTHDC1 RIP experiments will address this possibility and facilitate the elucidation of the mechanism underlying m6A-dependent regulation of A-P axis specification. We proposed a model in which YTHDC1 binds to the m6A sites at the 3′ UTR and CDS region to regulate the regeneration of the head and tail related wounds, respectively (Fig. S7c).

4. Conclusions

m6A methylation constitutes a novel layer of complexity in the regulation of gene expression in response to injury and plays a pivotal role in regeneration polarity. We describe, for the first time, the m6A RNA methylation landscape at a single base resolution in planarian *Dugesia japonica*, revealing a varying m6A level between the planarian fragments (head, trunk and tail) and a dynamic changes during regeneration. In addition, m6A methylation is enriched at the 3′ UTR and CDS regions of the transcripts in the head and tail fragments, respectively. Finally, we found that YTHDC1 serves as the primary m6A reader in planarian *Dugesia japonica*. The limitation of this study is that the samples are derived from whole planarian fragments rather than blastema, so the analysis results may be interfered by the original gene expression patterns of cells in non-regenerative tissues. These findings may hint at the potential role of m6A in regulating polarity and specification of the A-P axis during regeneration, though a further exploration is necessary in order to confirm the themes raised herein.

5. Materials and methods

5.1. Animals

A clonal strain of the planarian *Dugesia japonica*, originally obtained from Boshan, China, was established in our laboratory and used in all experiments. The *Dugesia japonica* planarians were cultured in Lushan spring water at 20 °C. Before use in experiments, all planarians were starved for at least 7 days. For the regeneration experiments, the planarian heads were removed and the fragments were used for experiments at 0, 1, 3, 5, 7, and 10 days after amputation.

5.2. Quantitative real-time PCR (qPCR)

Quantitative expressions of *Mettl3* and *Mettl14* were monitored using qPCR. *Mettl3* and *Mettl14* primers were designed by Primer Premier, version 5.0 (Table S1). The GAPDH gene was used as the internal reference. Briefly, total RNA from head, trunk, tail fragments at different time points (0, 1, 3, 5, 7, 10 d) following amputation were extracted with triol reagent (Invitrogrn, USA). The qPCR amplification was performed on the analytikjena qTower^3 G (Germany) using the ChamQ Universal SYBR qPCR Master Mix (Vazyme). Data were calculated using the $2^{-\triangle\triangle ct}$ method.

5.3. RNA interference (RNAi)

Double-stranded RNA (dsRNA) for *Mettl3*, *Mettl14* and *Ythdc1* was synthesized by PCR. The dsRNA-*Mettl3, Mettl14* and *Ythdc1* primers were designed using Primer Premier 5.0 (Table S1). dsRNA was synthesized in accordance with the manufacturer's instructions provided in the MEGAscriptTM RNAi Kit (Invitrogen, USA), and thereafter the planarian was soaked in 30 ng/μl dsRNA for 6 h and before being transfered to the culture medium. Control animals were soaked with the green fluoredrescent protein (GFP) dsRNA.

5.4. Immunofluorescent staining

Anti-m6A (SYSY, 202003)、Anti-METTL3 (Invitrogen, 72034)、Anti-METTL14 (CST, 51104)、Anti-YTHDC1 (Proteintech, 29441–1-AP) immunostaining were performed as previously described [38]. Briefly, the planarians were euthanized with 2 % of HCl and fixed in paraformaldehyde at 37 ℃ for 1 h, followed by dehydration with 100 % of methanol and incubation with the primary antibodies before overnight incubation with HRP labeled secondary antibodies (Thermo Fisher, A32790) at 4 ℃. Signals were examined and recorded with a laser confocal microscope.

5.5. Dot blot

In total, 200–500 ng total RNA from different tissues were spotted on a nylon N$^+$ membrane (GE Healthcare, RPN303B) and subjected to thermal cross-linking on a metal plate preheated to 70 °C. The membrane was then subjected to UV cross-linking twice at 2000 KJ followed by blocking in 5 % BSA for 1 h at room temperature. The membrane was then incubated with anti-m6A antibody (SYSY, 202 003) at 1:2000 for 2 h and washed thrice with 1 % TBST (Tris-buffered saline with 0.1 % Tween-20). It was then incubated with anti-rabbit antibody (diluted 1:5000, CST, 7074) for 1 h. After washing the membrane five times with 1 % TBST, a mixture of HRP substrates A and B (Thermo Fisher Scientific, 34095) were used for imaging. The membrane was then treated with a 1 % methylene blue solution for 3 min, washed with 1 % TBST and then visualized with a white light system.

5.6. mRNA-seq and m6A-REF-seq

mRNAs were purified from total RNAs using the Dynabeads® mRNA

purification kit (Ambion, 61006). cDNA libraries were made using the TruSeq RNA Sample Prep Kit (Illumina, FC-122–1001) in accordance with the manufacturer's instructions. All samples were sequenced by Illumina Nova-seq with paired-end 150 bp read length. The different library construction processes is shown in Fig. S3.

For m6A-REF-seq, the detail procedure is based on a published protocol [27]. An appropriate amount of RNA samples (~100 ng) was subjected to MazF digestion treatment. To perform MazF digestion, RNA samples were first denatured at 85 °C for 5 min and then chilled on ice for 2 min. Next, equivalent amounts of cellular mRNA were incubated with 1 μl MazF enzyme (20 U) and reaction buffer at 37 °C for 30 min. After RNA purification using the RNA Clean & Concentrator-5 kit (Zymo Research, R1015), the product was end repaired by T4 polynucleotide kinase (NEB, M0201S). Purified RNA fragments were finally subjected to NGS library construction using the VAHTS Small RNA Library Prep kit (Vazyme Biotech, NR801).

For IVT control library, the detail procedure is based on a published protocol [28]. The extracted 100 ng mRNA was first annealed with 1 μl poly(T) primer(12 μM) at 75 °C for 3 min and 42 °C for 2 min. Next, the first-strand cDNA was mixed by adding 2 μl 5 × first-strand buffer for SMARTScribe Reverse Transcriptase (Takara, 639536), 0.5 μl 100 mM dithiothreitol, 0.5 μl RNase inhibitor (Takara, 2313 A), 1 μl TSO T7 primer (10 μM), 1 μl 50 × Advantage UltraPure PCR Deoxynucleotide Mix (Takara, 639125) and 1 μl SMARTScribe Reverse Transcriptase (Takara, 639536). The first-strand cDNA mixture was added to the mRNA-poly (T) primer mixture, incubated at 42 °C for 1.5 h, and heated at 68 °C for 10 min for first-strand cDNA synthesis. After adding 10 μl 10 × Advantage 2 PCR buffer, 1 μl Advantage 2 PCR Polymerase Mix (Takara, 639207), 2 μl 50 ×Advantage UltraPure PCR Deoxynucleotide Mix, 2 μl T7 extension primer (10 μM), 2 μl RNase H (NEB, M0297) and RNase-free water to 100 μl, the primer extension reaction was conducted at 37 °C for 15 min, 95 °C for 2 min, 60 °C for 1 min and 68 °C for 10 min. Double-strand cDNA was purified using the NucleoSpin PCR clean-up kit (MACHEREY-NAGEL, 740609.50) or 1 × DNA beads (Vazyme Biotech, N411). The T7 transcription step was performed at 37 °C for 2 h using the HiScribe T7 High Yield RNA Synthesis kit (NEB, E2040) and NTPs from Takara Bio (6140). The sample was subjected to treatment with TURBO DNase (Thermo Fisher, AM2238) at 37 °C for 30 min to remove dsDNA and then purified with the RNA Clean & Concentrator-5 kit (Zymo Research, R1015). The concentration of IVT RNA was measured with the Qubit RNA HS Assay kit (Thermo Fisher, Q32852). m6A-REF-seq libraries were constructed from 100 ng cellular IVT RNA samples by using the VAHTS Small RNA Library Prep kit (Vazyme Biotech, NR801).

5.7. De novo assembly and transcriptome analysis

After adaptor trimming and filtering of low quality reads by fastp software (v0.20.0) [29], the resulting reads for the three fragments (head, trunk and tail) were merged into a single dataset and the TRINITY software (v2.8.5) was used to *de novo* assemble the reads into contigs [30]. To avoid redundant transcripts, the longest isoform for each "gene" as identified by TRINITY (unigene) was left with the "get_longest_isoform_seq_per_trinity_gene.pl'' utility in TRINITY. We assessed the assembly completeness in terms of gene content using BUSCO software (v5.3.0) by searching the unigenes for the presence or absence of conserved orthologs in the eukaryota_odb10 database [39].

We also mapped all the unigenes to the SwissProt database (ftp://ftp.ebi.ac.uk/pub/databases/uniprot/) and the NCBI non-redundant (nr) database (ftp://ftp.ncbi.nih.gov/blast/db/FASTA/nr.gz) using the diamond software (v2.0.14.152) with an E-value cutoff of 1e-5 [40]. We predicted protein-coding regions in the unigenes based on the most likely longest ORF using TransDecoder software (v5.5.0) (https://github.com/TransDecoder/TransDecode). The unigene expression was calculated with align_and_estimate_abundance.pl utility in TRINITY. Differentially expressed unigenes were filtered based on raw counts with

edgeR software (v3.16.5) between two samples or DESeq2 R packages (v1.31.0) between two groups of samples (P cutoff: 0.05, fold change cutoff: 2.0) [41,42]. Clusterprofiler R packages (v3.18.1) was used to perform the GO enrichment analysis based on the IDmapping databases and pathway enrichment analysis based on the KAAS auto annotation webserver (https://www.genome.jp/tools/kaas/) [43,44].

5.8. m6A-REF-seq data analysis

Based on the above assembled transcriptome, m6A sites were identified according to our previously publication [27]. Briefly, the m6A-REF-seq clean reads were mapped by the hisat2 software (v2.4.2) with default parameters [45]. m6A levels were calculated by the m6A ratio from m6A-REF-seq sample minus the m6A ratio from corresponding IVT sample with at least 10 read counts and a m6A level decreasing of 0.1. Mfuzz R packages was used to perform the time series analysis to show the methylated trend of different days [36]. Gene metaplot was plotted with Guitar R package (https://bioconductor.org/packages/release/bioc/html/Guitar.html).

5.9. Statistical Analysis

Results are presented as mean $\pm$ SD. Comparisons between groups were carried out using multiple t-tests. For all analyses, $*P < 0.05$, $**P < 0.01$ and $***P < 0.001$ were considered statistically significant. Statistical analyses were carried out using SPSS statistical software for Windows, version 16.0 (SPSS).

Ethics approval and consent to participate

Not applicable.

Consent for publication

Consent has been obtained from the participant for data publication.

CRediT authorship contribution statement

Liqian Chen: Conceptualization, Methodology, Visualization, Writing - original draft. Hui Zhen: Methodology, Writing - original draft. Zixin Chen: Formal analysis, Visualization. Mujie Huang: Methodology. Daniel W. Mak: Writing - original draft. Wei Jin: Writing - original draft. Yuxiu Zou: Resources. Mingjie Chen: Formal analysis, Visualization. Mingyue Zheng: Resources. Qingqiang Xie: Resources. Zhongjun Zhou: Conceptualization, Writing - original draft, Writing - review & editing, Supervision. Guoxiang Jin: Conceptualization, Writing - original draft, Writing - review & editing, Supervision. All authors read and approved the final manuscript.

Declaration of Competing Interest

The authors declare no competing interests.

Data Availability

All data generated for this paper have been deposited at NCBI's Gene Expression Omnibus under accession number GSE216412. Reviewers

can access the raw data using the token qhajskoyjnajdqf before publication.

Acknowledgements

Appendix A. Supporting information

Supplementary data associated with this article can be found in the online version at doi:10.1016/j.csbj.2023.09.018.

References

[1] Kimelman D, Martin BL. Anterior–posterior patterning in early development: three strategies. Wiley Interdiscip Rev: Dev Biol 2012;1(2):253–66.

[2] Carron C, Shi DL. Specification of anteroposterior axis by combinatorial signaling during Xenopus development. Wiley Interdiscip Rev: Dev Biol 2016;5(2):150–68.

[3] Reddien PW. The cellular and molecular basis for planarian regeneration. Cell 2018;175(2):327–45.

[4] Witchley JN, Mayer M, Wagner DE, Owen JH, Reddien PW. Muscle cells provide instructions for planarian regeneration. Cell Rep 2013;4(4):633–41.

[5] Scimone ML, Cote LE, Rogers T, Reddien PW. Two FGFRL-Wnt circuits organize the planarian anteroposterior axis. Elife 2016;5:e12845.

[6] Fincher CT, Wurtzel O, de Hoog T, Kravarik KM, Reddien PW. Cell type transcriptome atlas for the planarian Schmidtea mediterranea. Science 2018;360 (6391):eaaq1736.

[7] Cho Y, Sloutsky R, Naegle KM, Cavalli V. Injury-induced HDAC5 nuclear export is essential for axon regeneration. Cell 2013;155(4):894–908.

[8] Finelli MJ, Wong JK, Zou H. Epigenetic regulation of sensory axon regeneration after spinal cord injury. J Neurosci 2013;33(50):19664–76.

[9] Gaub P, Joshi Y, Wuttke A, Naumann U, Schnichels S, Heiduschka P, et al. The histone acetyltransferase p300 promotes intrinsic axonal regeneration. Brain 2011; 134(7):2134–48.

[10] Puttagunta R, Tedeschi A, Sória MG, Hervera A, Lindner R, Rathore KI, et al. PCAF-dependent epigenetic changes promote axonal regeneration in the central nervous system. Nat Commun 2014;5(1):1–13.

[11] Molinie B, Wang J, Lim KS, Hillebrand R, Lu ZX, Van Wittenberghe N, et al. m6A-LAIC-seq reveals the census and complexity of the m6A epitranscriptome. Nat Methods 2016;13(8):692–8.

[12] Dominissini D, Moshitch-Moshkovitz S, Schwartz S, Salmon-Divon M, Ungar L, Osenberg S, et al. Topology of the human and mouse m6A RNA methylomes revealed by m6A-seq. Nature 2012;485(7397):201–6.

[13] Liu J, Yue Y, Han D, Wang X, Fu Y, Zhang L, et al. A METTL3-METTL14 complex mediates mammalian nuclear RNA N6-adenosine methylation. Nat Chem Biol 2014;10(2):93–5.

[14] Ke S, Alemu EA, Mertens C, Gantman EC, Fak JJ, Mele A, et al. A majority of m6A residues are in the last exons, allowing the potential for 3′UTR regulation. Genes Dev 2015;29(19):2037–53.

[15] Meyer KD, Jaffrey SR. Rethinking m6A readers, writers, and erasers. Annu Rev Cell Dev Biol 2017;33:319–42.

[16] Jiang X, Liu B, Nie Z, Duan L, Xiong Q, Jin Z, et al. The role of m6A modification in the biological functions and diseases. Signal Transduct Target Ther 2021;6(1): 1–16.

[17] Wang M, Xiao Y, Li Y, Wang X, Qi S, Wang Y, et al. RNA m6A modification functions in larval development and caste differentiation in honeybee (Apis mellifera). Cell Rep 2021;34(1):108580.

[18] Zhang M, Zhai Y, Zhang S, Dai X, Li Z. Roles of N6-Methyladenosine (m6A) in stem cell fate decisions and early embryonic development in mammals. Front Cell Dev Biol 2020;8:782.

[19] Zhang M, Zhai Y, Zhang S, Dai X, Li Z. Roles of N6-Methyladenosine (m6A) in stem cell fate decisions and early embryonic development in mammals. Front Cell Dev Biol 2020;8:782.

[20] Weng YL, Wang X, An R, Cassin J, Vissers C, Liu Y, et al. Epitranscriptomic m6A regulation of axon regeneration in the adult mammalian nervous system. Neuron 2018;97(2):313–25.

[21] Cao X, Shu Y, Chen Y, Xu Q, Guo G, Wu Z, et al. Mettl14-mediated m6A modification facilitates liver regeneration by maintaining endoplasmic reticulum homeostasis. Cell Mol Gastroenterol Hepatol 2021;12(2):633–51.

[22] Xu Y, Zhou Z, Kang X, Pan L, Liu C, Liang X, et al. Mettl3-mediated mRNA m6A modification controls postnatal liver development by modulating the transcription factor Hnf4a. Nat Commun 2022;13(1):1–17.

[23] Gheller BJ, Blum JE, Fong EHH, Malysheva OV, Cosgrove BD, Thalacker-Mercer AE. A defined N6-methyladenosine (m6A) profile conferred by METTL3 regulates muscle stem cell/myoblast state transitions. Cell Death Discov 2020;6(1): 1–14.

[24] Liang Y, Han H, Xiong Q, Yang C, Wang L, Ma J, et al. METTL3-Mediated m6A methylation regulates muscle stem cells and muscle regeneration by notch signaling pathway. Stem Cells Int 2021;2021.

[25] Dagan Y, Yesharim Y, Bonneau AR, Frankovits T, Schwartz S, Reddien PW, et al. m6A is required for resolving progenitor identity during planarian stem cell differentiation. EMBO J 2022;41(21):e109895.

[26] Yang Y, Hsu PJ, Chen YS, Yang YG. Dynamic transcriptomic m6A decoration: writers, erasers, readers and functions in RNA metabolism. Cell Res 2018;28(6): 616–24.

[27] Zhang Z, Chen LQ, Zhao YL, Yang CG, Roundtree IA, Zhang Z, et al. Single-base mapping of m6A by an antibody-independent method. Sci Adv 2019;5(7): eaax0250.

[28] Zhang Z, Chen T, Chen HX, Xie YY, Chen LQ, Zhao YL, et al. Systematic calibration of epitranscriptomic maps using a synthetic modification-free RNA library. Nat Methods 2021;18(10):1213–22.

[29] Chen S, Zhou Y, Chen Y, Gu J. fastp: an ultra-fast all-in-one FASTQ preprocessor. Bioinformatics 2018;34(17):i884–90.

[30] Grabherr MG, Haas BJ, Yassour M, Levin JZ, Thompson DA, Amit I, et al. Full-length transcriptome assembly from RNA-Seq data without a reference genome. Nat Biotechnol 2011;29(7):644–52.

[31] Lence T, Akhtar J, Bayer M, Schmid K, Spindler L, Ho CH, et al. m6A modulates neuronal functions and sex determination in Drosophila. Nature 2016;540(7632): 242–7.

[32] Luo GZ, MacQueen A, Zheng G, Duan H, Dore LC, Lu Z, et al. Unique features of the m6A methylome in Arabidopsis thaliana. Nat Commun 2014;5(1):1–8.

[33] Wu Q, Hu Q, Hai Y, Li Y, Gao Y. METTL13 facilitates cell growth and metastasis in gastric cancer via an eEF1A/HN1L positive feedback circuit. J Cell Commun Signal 2023;17(1):121–35.

[34] Kershner L, Welshhans K. RACK1 regulates neural development. Neural Regen Res 2017;12(7):1036–9.

[35] Zhao T, Goh KJ, Ng HH, Vardy LA. A role for polyamine regulators in ESC self-renewal. Cell Cycle (Georget, Tex) 2012;11(24):4517–23.

[36] Kumar L, Futschik ME. Mfuzz: a software package for soft clustering of microarray data. Bioinformation 2007;2(1):5.

[37] Chen LQ, Zhao WS, Luo GZ. Mapping and editing of nucleic acid modifications. Comput Struct Biotechnol J 2020;18:661–7.

[38] Zhen H, Huang M, Zheng M, Gao L, Guo Z, Pang Q, et al. WTAP regulates stem cells via TRAF6 to maintain planarian homeostasis and regeneration. Int J Biol Macromol 2020;124932.

[39] Manni M, Berkeley MR, Seppey M, Simão FA, Zdobnov EM. BUSCO update: novel and streamlined workflows along with broader and deeper phylogenetic coverage for scoring of eukaryotic, prokaryotic, and viral genomes. Mol Biol Evol 2021;38 (10):4647–54.

[40] Buchfink B, Xie C, Huson DH. Fast and sensitive protein alignment using DIAMOND. Nat Methods 2015;12(1):59–60.

[41] Robinson MD, McCarthy DJ, Smyth GK. edgeR: a Bioconductor package for differential expression analysis of digital gene expression data. bioinformatics 2010;26(1):139–40.

[42] Love MI, Huber W, Anders S. Moderated estimation of fold change and dispersion for RNA-seq data with DESeq2. Genome Biol 2014;15(12):1–21.

[43] Yu G, Wang LG, Han Y, He QY. clusterProfiler: an R package for comparing biological themes among gene clusters. Omics: a J Integr Biol 2012;16(5):284–7.

[44] Moriya Y, Itoh M, Okuda S, Yoshizawa AC, Kanehisa M. KAAS: an automatic genome annotation and pathway reconstruction server. Nucleic Acids Res 2007;35 (suppl_2):W182–5.

[45] Kim D, Paggi JM, Park C, Bennett C, Salzberg SL. Graph-based genome alignment and genotyping with HISAT2 and HISAT-genotype. Nat Biotechnol 2019;37(8): 907–15.